Letter

Emergent Fano-Feshbach resonance in two-band superconductors with an incipient quasiflat band: Enhanced critical temperature evading particle-hole fluctuations

Hiroyuki Tajima,[1,2] Hideo Aoki,[1] Andrea Perali,[3] and Antonio Bianconi[4,5]

[1]*Department of Physics, Graduate School of Science, The University of Tokyo, Hongo, Tokyo 113-0033, Japan*

[2]*RIKEN Nishina Center (RNC), Wako, Saitama 351-0198, Japan*

[3]*School of Pharmacy, Physics Unit, Universitá di Camerino, 62032 Camerino (MC), Italy*

[4]*Rome International Center for Materials Science, Superstripes RICMASS, Via dei Sabelli 119A, 00185 Roma, Italy*

[5]*National Research Council, CNR, Institute of Crystallography, IC, Via Salaria Km 29 300, 00015 Monterotondo (Roma), Italy*

(Received 9 February 2024; revised 27 March 2024; accepted 27 March 2024; published 11 April 2024)

In superconductivity, a surge of interests in enhancing T_c is ever mounting, where a recent focus is toward multiband superconductivity. In T_c enhancements specific to two-band cases, especially around the Bardeen-Cooper-Schrieffer to Bose-Einstein condensate crossover considered here, we have to be careful about how quantum fluctuations affect the many-body states, i.e., particle-hole fluctuations suppressing the pairing for attractive interactions. Here, we explore how to circumvent the suppression by examining multichannel pairing interactions in two-band systems. With the Gor'kov-Melik-Barkhudarov (GMB) formalism for particle-hole fluctuations in a continuous space, we look into the case of a deep dispersive band accompanied by an incipient heavy-mass (i.e., quasiflat) band. We find that, while the GMB corrections usually suppress T_c significantly, this in fact competes with the enhanced pairing arising from the heavy band, with the trade-off leading to a *peaked* structure in T_c against the band-mass ratio when the heavy band is incipient. The system then plunges into a strong-coupling regime with the GMB screening vastly suppressed. This occurs prominently when the chemical potential approaches the bound state lurking just below the heavy band, which can be viewed as a Fano-Feshbach resonance, with its width governed by the pair-exchange interaction. The diagrammatic structure comprising particle-particle and particle-hole channels is heavily entangled, so that the emergent Fano-Feshbach resonance dominates all the channels, suggesting a universal feature in multiband superconductivity and superfluidity.

DOI: 10.1103/PhysRevB.109.L140504

Introduction. Multiband electronic systems and their multicomponent superconducting phases can harbor novel quantum effects. Superconductivity and its microscopic theory initiated by Bardeen, Cooper, and Schrieffer (BCS) give a conceptual impact on various research fields that encompass nuclear and particle physics as well [1–3]. Moreover, the discoveries of high-T_c superconductors, such as cuprates [4] and iron pnictides [5], have ignited renewed interests toward the realization of higher-temperature superconductivity.

Crucial factors for amplification of superconductivity are mainly twofold: the interparticle interaction and the electronic band structure. For an attractive interaction, the question is designing the ways to enhance the magnitude of the interaction for one-band cases. A pivotal factor then is the crossover from the BCS regime with loosely bound Cooper pairs to the Bose-Einstein condensation (BEC) regime with tightly bound pairs when the strength of the attraction is increased and/or the carrier density is reduced [6–9]. While it is difficult to control the interaction *in situ* in condensed matters, the BCS-BEC crossover was realized about two decades ago in ultracold Fermi gases near the Fano-Feshbach resonance [10–13]. Recently, the realization of solid-state systems in the BCS-BEC crossover regime has also been reported in FeSe superconductors [14–18], Li_xZrNCl [19,20], and organic superconductors [21] by tuning carrier densities.

If we go over to multiband superconductors and superfluids, the increased degrees of freedom can host diverse quantum phenomena [22]. For example, a multiband configuration with shallow and deep bands plays a crucial role typically in FeSe [23]. A remarkable feature of the multiband BCS-BEC crossover is a reduction of pairing fluctuations in the strong-coupling regime [24–27] which tends to suppress the superconducting critical temperature T_c. This screening effect is consistent with the observation of missing pseudogap in FeSe [28], whereas the pseudogap induced by pairing fluctuations is expected in the single-band BCS-BEC crossover [29–33]. Regarding the realization of strong-coupling systems, geometrical quantum confinement in the form of slabs or stripes causes interference between wave functions associated to different subbands, inducing superconducting shape resonances when the chemical potential is close to one of the subband bottom [34]. Moreover, an interband pair-exchange coupling in two-band systems leads to a kind of the Suhl-Kondo mechanism [35,36] which modifies the effective attraction in each band [37–39], so that this can be evoked for realizing the BCS-BEC crossover. Unconventional phase transitions have also been reported even in simple two-band models without complicated band structures nor impurities [40–45]. Such multiband characters may be further enhanced when the effective mass in the second band is heavy (flat or quasiflat band) [46]. Recently, a resonant enhancement of T_c in

a multiband system near a topological Lifshitz transition has also been studied in spin-orbit-coupled artificial superlattices [47–49].

The multiband BCS-BEC crossover has been studied intensively, but an important point about fluctuations is still unclear. Namely, in single-band models, the particle-hole fluctuations for attractive interactions, as formulated by Gork'ov-Melik-Barkhudarov (GMB) [50], significantly reduce T_c. Quantitatively, the GMB correction is known to reduce T_c in single-band systems by a factor $(4e)^{1/3} \simeq 2.2$ in the weak-coupling (BCS) limit [51]. Thus an imperative question is to find out how the GMB correction arises in two-band systems. This becomes crucial, in our view, when the second band is *incipient*, where the chemical potential μ is close to the bottom of the second band and the band starts to be occupied. Intuitively, this situation is expected to strongly affect the interaction via the pair-exchange coupling.

Recently, the evolution of T_c along the BCS-BEC crossover has been experimentally detected in a single-band ultracold system of atomic fermions [52]. By comparing with the theoretical prediction of the GMB, which was originally devised for the BCS regime but then extended to the BCS-BEC crossover in Ref. [51], the existence of the GMB correction and its evolution has indeed been experimentally confirmed, after 60 years of the pioneering GMB paper [50]. Thus the question of how the GMB correction on T_c discussed in Ref. [51] will behave in two-band models is of both fundamental and practical importance.

Motivated by these backgrounds, the present Letter theoretically explores the GMB screening effects on T_c in a two-band system consisting of a dispersive (light-mass) band and a quasiflat (heavy-mass) band with intraband attractive interactions accompanied by interband pair-exchange couplings. We focus on the situation where the heavy band is *incipient* (with the chemical potential close to the bottom of the second band) to fathom how the heavy band can dominate the dispersive band. For that, we have extended the GMB approach to two-band systems in terms of the simplified diagrammatic approach developed in Ref. [53]. In particular, the different effective masses of dispersive and quasiflat bands are considered here, in contrast to Ref. [23] where only equal-mass two bands were considered and hence the effects of the incipient quasiflat band were unraveled.

Two-band system composed of dispersive and quasiflat bands. We consider a two-band model in continuum in three dimensions described by the Hamiltonian

$$H = \sum_{\boldsymbol{k},\sigma,n} \xi_{\boldsymbol{k},n} c^\dagger_{\boldsymbol{k},\sigma,n} c_{\boldsymbol{k},\sigma,n} + \sum_{\boldsymbol{k},\boldsymbol{k}',\boldsymbol{q},n,n'} U_{nn'} b^\dagger_{\boldsymbol{k},\boldsymbol{q},n} b_{\boldsymbol{k}',\boldsymbol{q},n'}, \quad (1)$$

where $c^\dagger_{\boldsymbol{k},\sigma,n}$ creates a fermion with momentum $\boldsymbol{k}$ and spin $\sigma = \uparrow, \downarrow$ in band $n(= 1, 2)$, and $b^\dagger_{\boldsymbol{k},\boldsymbol{q},n} \equiv c^\dagger_{\boldsymbol{k}+\boldsymbol{q}/2,\uparrow,n} c^\dagger_{-\boldsymbol{k}+\boldsymbol{q}/2,\downarrow,n}$ is a pair-creation operator. $\xi_{\boldsymbol{k},n} = \varepsilon_{\boldsymbol{k},n} - \mu + E_0\delta_{n,2}$ is the kinetic energy in band n measured from the chemical potential μ, where $\varepsilon_{\boldsymbol{k},n} = k^2/2m_n$ (m_n is the effective mass of band n) and E_0 is the band offset between the two bands [see Fig. 1(a)]. In this work, we assume that the upper band ($n = 2$) has a heavier effective mass, $m_2 \geqslant m_1$.

To characterize the intraband interaction strength U_{nn}, we use a scattering length a_{nn} given by $\frac{m_n}{4\pi a_{nn}} = U_{nn}^{-1} + \frac{m_n \Lambda}{2\pi^2}$ for

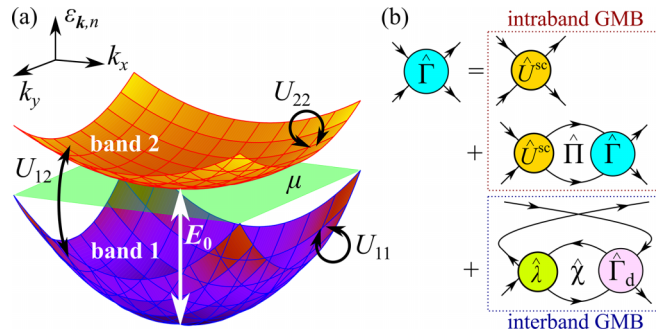

FIG. 1. (a) The band structure of the two-band model considered here with a light-mass first band and a heavy-mass second band with intraband (U_{11}, U_{22}) and interband ($U_{12} = U_{21}$) couplings, and the band offset E_0. The chemical potential μ is set to be close to the bottom of the second band. (b) Diagrammatic representation of the many-body T matrix $\hat{\Gamma}$ in the GMB formalism that comprises the intraband interaction through the screened coupling $\hat{U}^{\rm sc}$ (encircled in red), and the GMB correction for the interband pair-exchange interaction through the pair-exchange-induced coupling $\hat{\lambda}$ and the diagonal component $\hat{\Gamma}_{\rm d}$ (encircled in blue).

$n = 1, 2$, where Λ is the momentum cutoff that is needed in continuum models [40]. We can roughly translate Λ as the bandwidth in lattice models. For simplicity, we assume that the intraband interaction is independent of the band index, $U_{22} = U_{11}$. The coupling U_{11} within the dispersive band is kept weak in such a way that the corresponding scattering length is negative, $k_0 a_{11} = -1.0$ here. The interband pair-exchange couplings are U_{12} and U_{21} (=U_{21} for the Hermiticity of H). It is convenient to introduce a dimensionless coupling as $\tilde{U}_{12} \equiv U_{12}\frac{\sqrt{m_1 m_2}k_0}{2\pi^2} = \tilde{U}_{21}$, where we have introduced a momentum scale $k_0 \equiv \sqrt{2m_1 E_0}$.

Many-body T matrix with particle-hole fluctuations. Let us now present the equation for T_c with the GMB screening effect in the present two-band system based on the diagrammatic approach. As displayed in Fig. 1(b), the many-body T matrix $\hat{\Gamma}$ in the 2×2 matrix representation for band indices reads

$$\hat{\Gamma}(q) = \hat{U}^{\rm sc} - \hat{U}^{\rm sc}\hat{\Pi}(q)\hat{\Gamma}(q) - \hat{\lambda}(q)\langle\hat{\chi}\rangle\hat{\Gamma}_{\rm d}(q), \quad (2)$$

where $q = (\boldsymbol{q}, i\nu_\ell)$ is the four-momentum index with boson Matsubara frequency $\nu_\ell = 2\pi\ell T$ ($\ell \in \mathbb{Z}$), and

$$\hat{U}^{\rm sc} = \begin{pmatrix} U_{11}^{\rm sc} & U_{12} \\ U_{21} & U_{22}^{\rm sc} \end{pmatrix} \quad (3)$$

is the coupling constant matrix. Its diagonal components involve the GMB screening for U_{11} and U_{22} as $U_{nn}^{\rm sc} = U_{nn}/(1 + U_{nn}\langle\chi_{nn}\rangle)$ with the averaged particle-hole bubble $\langle\chi_{nn}\rangle$ [53]. Here, we have simplified the framework following Ref. [51], which should be qualitatively valid, as indicated by T_c in Ref. [53] being similar to Ref. [51] across the BCS-BEC crossover. For $\mu - E_0\delta_{n,2} > 0$, we obtain

$$\langle\chi_{nn}\rangle = \frac{m_n}{4\pi^2}\int_{-1}^{1} ds \int_0^\infty \frac{kdk}{q_n} f(\xi_{\boldsymbol{k},n}) \ln\left|\frac{q_n - 2k}{q_n + 2k}\right|, \quad (4)$$

where we have defined $q_n \equiv \sqrt{2m_n(\mu - E_0\delta_{n,2})(1 + s)}$ and the Fermi distribution function $f(\xi_{\boldsymbol{k},n}) = (e^{\xi_{\boldsymbol{k},n}/T} + 1)^{-1}$. When $\mu - E_0\delta_{n,2} < 0$ where the Fermi surface is absent for

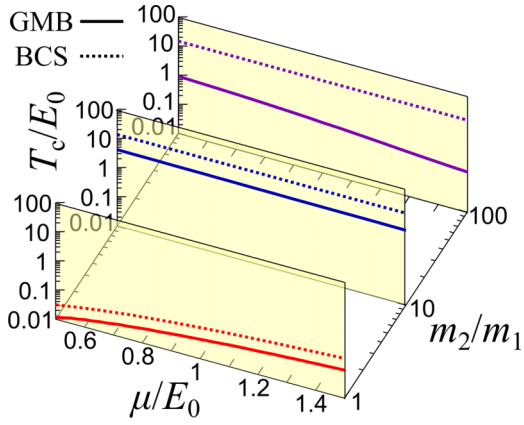

FIG. 2. Superconducting critical temperature T_c against the effective mass ratio m_2/m_1 and chemical potential μ/E_0 at $\tilde{U}_{12} = 10^{-3}$ and $\Lambda/k_0 = 10$. The solid and dotted curves show the GMB and BCS results, respectively.

band n, we get $\langle \chi_{nn} \rangle = -\frac{m_n}{2\pi^2} \int_0^\infty dk f(\xi_{\boldsymbol{k},n})$. This treatment reflects an aspect that the particle-hole bubble is strongly suppressed in the BEC regime, where the chemical potential strongly deviates from the Fermi energy that in the weak-coupling limit is given by $E_{\mathrm{F},n} = \frac{(3\pi^2\rho_n)^{2/3}}{2m_n}$ for a given number density ρ_n [25] and can become negative [51,53], leading to a progressively exponential suppression of the particle-hole bubble of the GMB correction. In Eq. (2), $\hat{\Pi}(q) = \mathrm{diag}[\Pi_{11}(q), \Pi_{22}(q)]$ is the particle-particle bubble with

$$\Pi_{nn}(q) = -\sum_{\boldsymbol{k}} \frac{1 - f(\xi_{\boldsymbol{k}+\boldsymbol{q},n}) - f(\xi_{-\boldsymbol{k},n})}{i\nu_\ell - \xi_{\boldsymbol{k}+\boldsymbol{q},n} - \xi_{-\boldsymbol{k},n}}. \tag{5}$$

The very last term of Eq. (2) [Fig. 1(b), bottom line] represents the GMB correction [see Fig. 1(b)], which consists of the pair-exchange-induced coupling $\hat{\lambda}(q) = \mathrm{diag}[-U_{12}U_{21}\Pi_{22}(q), -U_{12}U_{21}\Pi_{11}(q)]$, along with the particle-hole bubble $\langle \hat{\chi} \rangle \equiv \mathrm{diag}(\langle \chi_{11} \rangle, \langle \chi_{22} \rangle)$ and the diagonal component of the T matrix, $\Gamma_{\mathrm{d}}(q) = \mathrm{diag}[\Gamma_{11}(q), \Gamma_{22}(q)]$, so that particle-particle and particle-hole channels are heavily entangled. Based on the Thouless criterion [54], T_c is obtained where $[\Gamma_{ij}(q=0)]^{-1} = 0$ is achieved [25,26]. For details about the formalism, see Supplemental Material [55].

Interplay between pairing and particle-hole fluctuations. Let us now present the numerical result for the superconducting critical temperature T_c incorporating the GMB correction in Fig. 2, where the pair-exchange coupling is set to be $\tilde{U}_{12} = 10^{-3}$ (we frequently employ this value to discuss the effect of heavy mass m_2 in the main text; for different $\tilde{U}_{12}$, see Supplemental Material [55]). For comparison, the BCS result without the GMB correction is also displayed. Large enhancements in T_c can be found for large $m_2/m_1 = 10, 100$, particularly in BCS but also for GMB. In the limit of $m_2/m_1 \to \infty$, the Thouless criterion without the GMB correction simplifies to [55]

$$1 + \frac{U_{22}^{\mathrm{eff}}\Lambda^3}{6\pi^2}\mathcal{F}(E_0 - \mu) = 0, \tag{6}$$

where $U_{22}^{\mathrm{eff}} \equiv U_{22} - U_{12}\Pi_{11}(0)U_{21}/[1 + U_{11}\Pi_{11}(0)]$, and we have defined $\mathcal{F}(x) \equiv \frac{\tanh(x/2T_c)}{2x}$, which exhibits a maximum at $x = 0$ (i.e., $\mu = E_0$). In this limit, Eq. (6) can be easily satisfied around $\mu = E_0$ even for small U_{11} and U_{22} for sufficiently large Λ. While this fact is reminiscent of the enhanced pairing near the Lifshitz transition around a van Hove singularity, the BCS result with larger m_2/m_1 in Fig. 2 shows a weak μ dependence because the width of $\mathcal{F}(E_0 - \mu)$ is $\sim T_c/E_0$ ($\simeq$14 here). We note that the strong enhancement of T_c/E_0 is associated with the cutoff-dependent effective interaction $U_{22}^{\mathrm{eff}}\Lambda^3$ in Eq. (6). In other words, T_c depends on how far the quasiflat dispersion extends in the momentum space in band 2.

If we turn to the GMB result (solid lines in Fig. 2), we find that the GMB correction significantly reduces T_c from the BCS result, particularly for large m_2/m_1. This comes from the particle-hole bubble $\langle \chi_{22} \rangle$, which blows up for large m_2/m_1. For $\mu - E_0 \leqslant 0$, we have an expression

$$\langle \chi_{22} \rangle = \frac{m_2\sqrt{2\pi m_2 T_c}}{4\pi^2}\mathrm{Li}_{1/2}(-z), \tag{7}$$

where $z = e^{(\mu - E_0)/T_c}$ is an effective fugacity and $\mathrm{Li}_s(x)$ is the polylogarithm. Specifically, for $\mu \to E_0$ (i.e., $z \to 1$), we have $\langle \chi_{22} \rangle = -\frac{m_2\sqrt{2\pi m_2 T_c}}{4\pi^2}(1 - \sqrt{2})\zeta(1/2)$ with the Riemann zeta function $\zeta(1/2) \simeq -1.46$. This leads to a divergent behavior of $\langle \chi_{22} \rangle \propto m_2^{3/2}$ for $m_2 \to \infty$. Such a tendency persists for $\mu > E_0$ as seen in Fig. 2.

A notable feature in Fig. 2 is that T_c is much larger for $m_2/m_1 \gtrsim 10$ than for $m_2/m_1 \simeq 1$ even with the strong GMB reduction. Let us examine this more closely in Fig. 3(a1), which compares the m_2/m_1 dependence of T_c between BCS and GMB at $\mu/E_0 = 0.6$ with $\tilde{U}_{12} = 10^{-3}$. While the BCS result has the saturation of T_c at larger m_2/m_1 as expected from Eq. (6), the GMB result exhibits a *peak* of T_c around a finite $m_2/m_1 = 3.5$, beyond which T_c decreases monotonically with m_2/m_1. We can interpret the remarkable result as signifying a *competition* between the enhanced pairing due to the strong attraction in Eq. (6) and the strong GMB reduction. The trade-off results in an optimal mass ratio, which depends on the momentum cutoff ($\sim$bandwidth in lattice models) in the incipient heavy band, but the peaked structure persists when Λ is varied; see Supplemental Material [55]. To accurately evaluate the cutoff dependence, we would have to adopt some kind of renormalization scheme, which will be an interesting future work. We note that T_c does not exhibit a peak in the μ/E_0 dependence as shown in Fig. 3(a2).

Suppressed particle-hole fluctuations near the Fano-Feshbach resonance. We can further capture the behavior of T_c in terms of an underlying resonance. For that, let us look at the ratio $T_c^{\mathrm{GMB}}/T_c^{\mathrm{BCS}}$ between BCS and GMB schemes in Figs. 3(b1) and 3(b2). This ratio measures the extent to which the GMB screening is at work. In both of m_2/m_1 and μ/E_0 dependencies, $T_c^{\mathrm{GMB}}/T_c^{\mathrm{BCS}}$ exhibits a peaked behavior. Around $m_2/m_1 = 1.0$, one can find $T_c^{\mathrm{GMB}}/T_c^{\mathrm{BCS}} \simeq 0.4$ (for $k_0 a_{11} = -1.0$ here) regardless of the value of $\tilde{U}_{12}$, which originates from the GMB screening associated with the Fermi surface in band 1. Similar values $T_c^{\mathrm{GMB}}/T_c^{\mathrm{BCS}} \simeq 0.4$–$0.5$ are reported for $k_{\mathrm{F}}|a| < 1.0$ in a single-band study [51].

As m_2/m_1 is increased, we have a conspicuous peak of $T_c^{\mathrm{GMB}}/T_c^{\mathrm{BCS}}$, after which T_c^{GMB} starts to decrease because of enhanced particle-hole fluctuations for larger m_2/m_1, and the

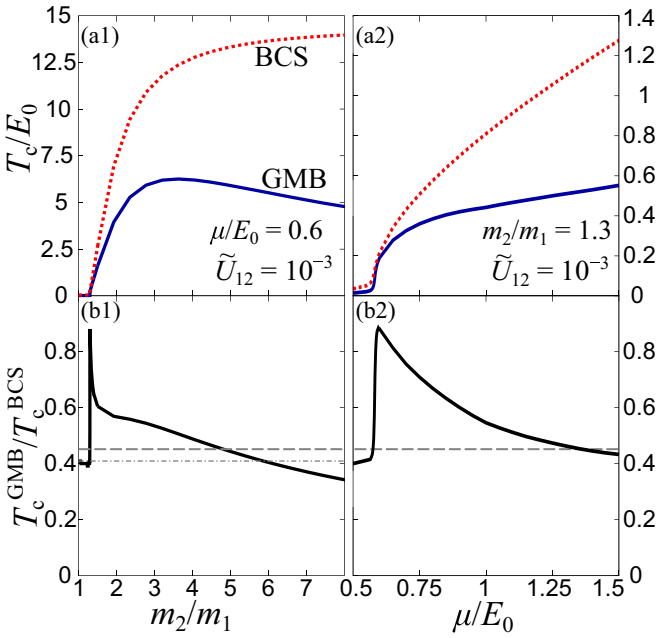

FIG. 3. (a1) Superconducting critical temperatures T_c as a function of the effective mass ratio m_2/m_1 at $\mu/E_0 = 0.6$. (a2) shows μ/E_0 dependence of T_c at $m_2/m_1 = 1.3$. $\tilde{U}_{12} = 10^{-3}$ and $\Lambda/k_0 = 10$. For comparison, the dotted curves show the BCS results without the GMB correction. The lower panels represent the ratio between the superconducting critical temperatures with and without the GMB corrections as functions of (b1) m_2/m_1 at $\mu/E_0 = 0.6$ and (b2) μ/E_0 at $m_2/m_1 = 1.3$. The horizontal dashed line indicates the ratio $(4e)^{-1/3} \simeq 0.45$ in the single-band counterpart at weak coupling. The value at $m_2/m_1 = 1$ is marked with the horizontal thin chain-dotted line in (b1).

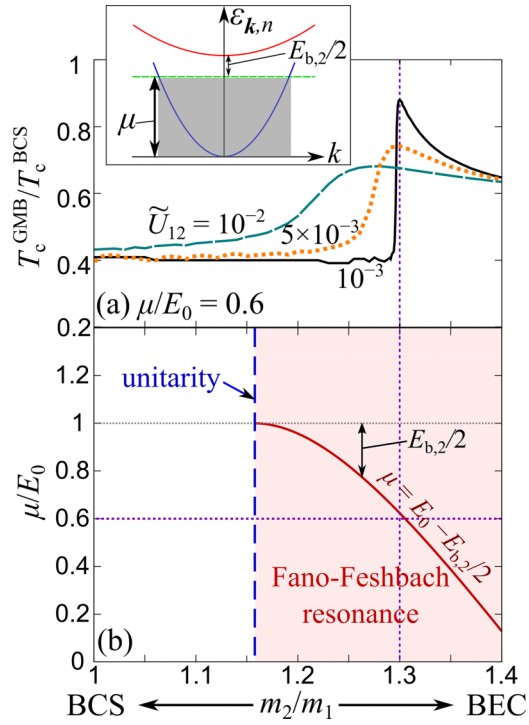

FIG. 4. (a) Calculated T_c^{GMB}/T_c^{BCS} as a function of m_2/m_1 with $\tilde{U}_{12} = 10^{-2}$, 5×10^{-3}, and 10^{-3} at $\mu/E_0 = 0.6$. The inset shows the schematics for single-particle energy level with the chemical potential μ touching the Fano-Feshbach resonance associated with the incipient heavy band. (b) Fano-Feshbach resonance line $\mu = E_0 - E_{b,2}/2$ at the weak interband coupling limit ($U_{12} \to 0$). The vertical blue line indicates the unitarity at which the two-body bound state appears in band 2. One can regard that the BCS (BEC) regime is realized in band 2 when m_2/m_1 is small (large). Purple lines mark the case of $\mu/E_0 = 0.6$ considered in (a).

ratio eventually drops below the single-band GMB result at weak coupling given by $(4e)^{-1/3} \simeq 0.45$. Nevertheless, the GMB reduction for larger m_2/m_1 is not drastic, indicating that the enhanced pairing effect is still remarkable at $m_2/m_1 \gtrsim 10$. Thus, even in the presence of the GMB correction, T_c remains large at $m_2/m_1 \gtrsim 10$ as compared to the case for $m_2/m_1 \simeq 1$ in Fig 3(a1).

Now, let us analyze the peak in T_c^{GMB}/T_c^{BCS} against m_2/m_1 in Fig. 4(a) for various values of $\tilde{U}_{12} = 10^{-3}$, 5×10^{-3}, and 10^{-2} at $\mu/E_0 = 0.6$. When m_2/m_1 increased from 1, a sharp enhancement of T_c^{GMB}/T_c^{BCS} emerges, especially at $\tilde{U}_{12} = 10^{-3}$ in Fig. 4(a), which indicates that the GMB correction on T_c is dramatically reduced there. The peak starts to be smeared for larger $\tilde{U}_{12}$.

Another notable feature is that the peak has an asymmetric shape in Fig. 4(a), which we can immediately recognize as reminiscent of the Fano-Feshbach resonance. Indeed, physics behind the dramatic reduction of the GMB correction on T_c for $\mu/E_0 < 1.0$ and smaller $\tilde{U}_{12}$ revealed in Fig. 4(a) should be a consequence of the chemical potential touching the incipient heavy band, thereby causing a Fano-Feshbach resonance in the following sense. The heavy band accommodates a bound state (which turns into the resonance state for nonzero $\tilde{U}_{12}$) for $m_2/m_1 \geqslant 1 - \frac{\pi}{2a_{11}\Lambda}$ ($\simeq$1.16 for the present choice of $k_0 a_{11} = -1.0$ and $\Lambda/k_0 = 10$) [55]. $m_2/m_1 \simeq 1.16$ can be regarded as the unitarity, [32,33] and the geometrical control of m_2/m_1, e.g., by band engineering with quantum confinement or orbital selection, leads to the BCS-BEC crossover as indicated in Fig. 4(b). For small U_{12}, the resonance energy ω_{res} is given by

$$\omega_{res} = -E_{b,2} + 2E_0 + O(U_{12}^4), \tag{8}$$

where $E_{b,2}$ is the two-body binding energy [inset of Fig. 4(a)] in band 2 for $U_{12} \to 0$. We can see that the peak of T_c^{GMB}/T_c^{BCS} for $\tilde{U}_{12} = 10^{-3}$ and $\mu/E_0 < 1.0$ does indeed take place at the mass ratio at which the Fano-Feshbach resonance resides, whose position shifts as μ/E_0 is varied. Namely, the resonance arises at $\mu = \omega_{res}/2 \simeq E_0 - E_{b,2}/2$ (with 1/2 for putting the two-body energy into the one per particle).

We have actually plotted in Fig. 4(b) the trajectory $\mu = E_0 - E_{b,2}/2$ against m_2/m_1 as the Fano-Feshbach resonance line. We can see that the sharp reduction of the GMB correction occurs right at the resonance. Both the bound state and the resonance start to exist above the unitarity mass ratio $m_2/m_1 = 1 - \frac{\pi}{2a_{11}\Lambda}$ [55] where the two-body bound state appears in band 2. When $E_{b,2}$ arises, as depicted schematically in Fig. 4(a) and marked with a double arrow in Fig. 4(b), electrons primarily occupy the resonant state, while the second band is basically empty for $\mu - E_0 < 0$ (except for thermally excited quasiparticles). In such a case, the heavy

band is in an extremely dilute (i.e., strong-coupling) regime characterized by $(\mu - E_0)/E_{b,2} \simeq -1/2$, which is a counterpart to the single-band expression, $\mu/E_b = -1/2$, for the chemical potential in the BEC limit (with E_b being the binding energy in the single-band case). The realization of the strong-coupling limit and the verge of appearance of the second-band Fermi surface, taking place around the Fano-Feshbach resonance at $\mu = E_0 - E_{b,2}/2$, thus lead to the suppression of the GMB screening effect.

Summary. We have investigated the GMB screening effect on the superconducting critical temperature in a two-band superconductor consisting of a deep dispersive (light-mass) band and a heavy-mass band with the chemical potential adjusted to make the heavy band incipient. By developing the diagrammatic GMB formalism for two-band systems, we have calculated the superconducting critical temperature T_c for various values of (i) the mass ratio of the two bands, (ii) chemical potential, and (iii) the pair-exchange coupling. A strong reduction of T_c, which we traced back to extremely large particle-hole fluctuations when the second band has a heavy mass, is found to be overcome, because the GMB reduction has to *compete* with the enhanced pairing interaction arising from the incipient heavy band, resulting in a *peaked* structure in T_c versus the mass ratio. We have then unraveled that there indeed exists a Fano-Feshbach resonance that occurs when the chemical potential traverses the energy of the two-body bound state emerging below the heavy band (which becomes a resonant state in the presence of the interband pair exchange). The GMB diagram is strongly suppressed when the Fermi surface of the incipient heavy band is collapsed because of the bound state leading to the Fano-Feshbach resonance. Thus we end up with a mechanism for evading the screening effects of particle-hole (GMB) fluctuations, leaving the critical temperature in a protectorate regime of parameters.

The present results are expected to give a hint for further understanding of many-body physics in multicomponent condensations as well as material design toward high-T_c superconductors with band or structure engineering such as superlattices. As a future perspective, it would be interesting to go beyond the present approach by incorporating the full momentum and energy dependence of the particle-hole diagrams and the Popov correction for interacting molecular pairs, following the approach of Ref. [51]. The effects of spin-orbit coupling may also be important in applying the present approach to topological superconductors with Rashba heterostructures [47]. We can mention in passing that, in lattice systems where the particle-hole transformation can be applied in certain conditions, it could be possible, through the attraction-repulsion transformation, to clarify the relevance of the present scheme to the repulsive multiband systems where spin fluctuations are dominant [56–62]. Lattices also make the introduction of cutoffs unnecessary, which will facilitate the diagrammatic analysis. It is also worth studying the role of the low dimensionality such as the GMB effect on the Berezinskii-Kosterlitz-Thouless transition [63–65] and on the behavior of the suppression coefficient of the mean-field pairing temperature for two-dimensional systems, which are of considerable interest.

Acknowledgments. H.T. thanks Y. Yerin, P. Pieri, K. Ochi, K. Iida, and H. Liang's group at the University of Tokyo for useful discussions. H.T. was supported by the JSPS Grants-in-Aid for Scientific Research under Grants No. JP18H05406, No. JP22H01158, and No. JP22K13981. H.A. thanks CREST (Grant No. JPMJCR18T4). A.P. was supported by PNRR MUR Project No. PE0000023-NQSTI.

[1] A. Bohr, B. R. Mottelson, and D. Pines, Phys. Rev. **110**, 936 (1958).
[2] Y. Nambu and G. Jona-Lasinio, Phys. Rev. **122**, 345 (1961).
[3] Y. Nambu and G. Jona-Lasinio, Phys. Rev. **124**, 246 (1961).
[4] J. G. Bednorz and K. A. Müller, Z. Phys. B **64**, 189 (1986).
[5] Y. Kamihara, T. Watanabe, M. Hirano, and H. Hosono, J. Am. Chem. Soc. **130**, 3296 (2008).
[6] D. M. Eagles, Phys. Rev. **186**, 456 (1969).
[7] A. J. Leggett, *Modern Trends in the Theory of Condensed Matter: Proceedings of the XVI Karpacz Winter School of Theoretical Physics, 1979, Karpacz, Poland* (Springer, Berlin, 2008), pp. 13–27.
[8] P. Nozières and S. Schmitt-Rink, J. Low Temp. Phys. **59**, 195 (1985).
[9] C. A. R. Sá de Melo, M. Randeria, and J. R. Engelbrecht, Phys. Rev. Lett. **71**, 3202 (1993).
[10] C. Chin, R. Grimm, P. Julienne, and E. Tiesinga, Rev. Mod. Phys. **82**, 1225 (2010).
[11] C. A. Regal, M. Greiner, and D. S. Jin, Phys. Rev. Lett. **92**, 040403 (2004).
[12] M. W. Zwierlein, C. A. Stan, C. H. Schunck, S. M. F. Raupach, A. J. Kerman, and W. Ketterle, Phys. Rev. Lett. **92**, 120403 (2004).
[13] M. Bartenstein, A. Altmeyer, S. Riedl, S. Jochim, C. Chin, J. H. Denschlag, and R. Grimm, Phys. Rev. Lett. **92**, 203201 (2004).
[14] Y. Lubashevsky, E. Lahoud, K. Chashka, D. Podolsky, and A. Kanigel, Nat. Phys. **8**, 309 (2012).
[15] S. Kasahara, T. Watashige, T. Hanaguri, Y. Kohsaka, T. Yamashita, Y. Shimoyama, Y. Mizukami, R. Endo, H. Ikeda, K. Aoyama *et al.*, Proc. Natl. Acad. Sci. USA **111**, 16309 (2014).
[16] S. Rinott, K. B. Chashka, A. Ribak, E. D. L. Rienks, A. Taleb-Ibrahimi, P. L. Fevre, F. Bertran, M. Randeria, and A. Kanigel, Sci. Adv. **3**, e1602372 (2017).
[17] T. Hashimoto, Y. Ota, A. Tsuzuki, T. Nagashima, A. Fukushima, S. Kasahara, Y. Matsuda, K. Matsuura, Y. Mizukami, T. Shibauchi, S. Shin, and K. Okazaki, Sci. Adv. **6**, eabb9052 (2020).
[18] Y. Mizukami, M. Haze, O. Tanaka, K. Matsuura, D. Sano, J. Böker, I. Eremin, S. Kasahara, Y. Matsuda, and T. Shibauchi, Commun. Phys. **6**, 183 (2023).
[19] Y. Nakagawa, Y. Saito, T. Nojima, K. Inumaru, S. Yamanaka, Y. Kasahara, and Y. Iwasa, Phys. Rev. B **98**, 064512 (2018).
[20] Y. Nakagawa, Y. Kasahara, T. Nomoto, R. Arita, T. Nojima, and Y. Iwasa, Science **372**, 190 (2021).

[21] Y. Suzuki, K. Wakamatsu, J. Ibuka, H. Oike, T. Fujii, K. Miyagawa, H. Taniguchi, and K. Kanoda, Phys. Rev. X **12**, 011016 (2022).
[22] M. V. Milošević and A. Perali, Supercond. Sci. Technol. **28**, 060201 (2015).
[23] A. V. Chubukov, I. Eremin, and D. V. Efremov, Phys. Rev. B **93**, 174516 (2016).
[24] L. Salasnich, A. A. Shanenko, A. Vagov, J. A. Aguiar, and A. Perali, Phys. Rev. B **100**, 064510 (2019).
[25] H. Tajima, Y. Yerin, A. Perali, and P. Pieri, Phys. Rev. B **99**, 180503(R) (2019).
[26] H. Tajima, Y. Yerin, P. Pieri, and A. Perali, Phys. Rev. B **102**, 220504(R) (2020).
[27] T. T. Saraiva, P. J. F. Cavalcanti, A. Vagov, A. S. Vasenko, A. Perali, L. Dell'Anna, and A. A. Shanenko, Phys. Rev. Lett. **125**, 217003 (2020).
[28] T. Hanaguri, S. Kasahara, J. Böker, I. Eremin, T. Shibauchi, and Y. Matsuda, Phys. Rev. Lett. **122**, 077001 (2019).
[29] A. Perali, P. Pieri, G. C. Strinati, and C. Castellani, Phys. Rev. B **66**, 024510 (2002).
[30] Q. Chen, J. Stajic, S. Tan, and K. Levin, Phys. Rep. **412**, 1 (2005).
[31] E. J. Mueller, Rep. Prog. Phys. **80**, 104401 (2017).
[32] G. C. Strinati, P. Pieri, G. Röpke, P. Schuck, and M. Urban, Phys. Rep. **738**, 1 (2018).
[33] Y. Ohashi, H. Tajima, and P. van Wyk, Prog. Part. Nucl. Phys. **111**, 103739 (2020).
[34] D. Innocenti, N. Poccia, A. Ricci, A. Valletta, S. Caprara, A. Perali, and A. Bianconi, Phys. Rev. B **82**, 184528 (2010).
[35] H. Suhl, B. T. Matthias, and L. R. Walker, Phys. Rev. Lett. **3**, 552 (1959).
[36] J. Kondo, Prog. Theor. Phys. **29**, 1 (1963).
[37] K. Nishiguchi, K. Kuroki, R. Arita, T. Oka, and H. Aoki, Phys. Rev. B **88**, 014509 (2013).
[38] C. Yue, H. Aoki, and P. Werner, Phys. Rev. B **106**, L180506 (2022).
[39] K. Ochi, H. Tajima, K. Iida, and H. Aoki, Phys. Rev. Res. **4**, 013032 (2022).
[40] M. Iskin and C. A. R. Sá de Melo, Phys. Rev. B **74**, 144517 (2006).
[41] M. Silaev and E. Babaev, Phys. Rev. B **84**, 094515 (2011).
[42] M. Silaev and E. Babaev, Phys. Rev. B **85**, 134514 (2012).
[43] L. Komendová, Y. Chen, A. A. Shanenko, M. V. Milošević, and F. M. Peeters, Phys. Rev. Lett. **108**, 207002 (2012).
[44] Y. Yerin, H. Tajima, P. Pieri, and A. Perali, Phys. Rev. B **100**, 104528 (2019).
[45] G. Midei and A. Perali, Phys. Rev. B **107**, 184501 (2023).
[46] H. Aoki, J. Supercond. Novel Magn. **33**, 2341 (2020).
[47] M. V. Mazziotti, A. Valletta, R. Raimondi, and A. Bianconi, Phys. Rev. B **103**, 024523 (2021).
[48] M. V. Mazziotti, A. Bianconi, R. Raimondi, G. Campi, and A. Valletta, J. Appl. Phys. **132**, 193908 (2022).
[49] G. Logvenov, N. Bonmassar, G. Christiani, G. Campi, A. Valletta, and A. Bianconi, Condens. Matter **8**, 78 (2023).
[50] L. P. Gor'kov and T. K. Melik-Barkhudarov, Zh. Eksp. Teor. Fiz. **40**, 1452 (1961) [Sov. Phys. JETP **13**, 1018 (1961)].
[51] L. Pisani, A. Perali, P. Pieri, and G. C. Strinati, Phys. Rev. B **97**, 014528 (2018).
[52] M. Link, K. Gao, A. Kell, M. Breyer, D. Eberz, B. Rauf, and M. Köhl, Phys. Rev. Lett. **130**, 203401 (2023).
[53] Z.-Q. Yu, K. Huang, and L. Yin, Phys. Rev. A **79**, 053636 (2009).
[54] D. J. Thouless, Ann. Phys. **10**, 553 (1960).
[55] See Supplemental Material at http://link.aps.org/supplemental/10.1103/PhysRevB.109.L140504 for details of the theoretical framework and additional numerical results for different values of parameters.
[56] H. Aoki and K. Kuroki, Phys. Rev. B **42**, 2125 (1990).
[57] K. Kuroki and H. Aoki, Phys. Rev. Lett. **69**, 3820 (1992).
[58] K. Kuroki and H. Aoki, Phys. Rev. B **48**, 7598 (1993).
[59] Mixed particle-particle and particle-hole diagrams have been evoked in a different context and formulated as the dynamical vertex approximation for repulsive lattice models in M. Kitatani, T. Schäfer, H. Aoki, and K. Held, Phys. Rev. B **99**, 041115(R) (2019).
[60] S. Sayyad, E. W. Huang, M. Kitatani, M.-S. Vaezi, Z. Nussinov, A. Vaezi, and H. Aoki, Phys. Rev. B **101**, 014501 (2020).
[61] S. Sayyad, M. Kitatani, A. Vaezi, and H. Aoki, J. Phys.: Condens. Matter **35**, 245605 (2023).
[62] K. Yamazaki, M. Ochi, D. Ogura, K. Kuroki, H. Eisaki, S. Uchida, and H. Aoki, Phys. Rev. Res. **2**, 033356 (2020).
[63] J. M. Kosterlitz, Rep. Prog. Phys. **79**, 026001 (2016).
[64] G. Midei, K. Furutani, L. Salasnich, and A. Perali, arXiv:2403.03025.
[65] S. K. Paramasivam, S. P. Gangadharan, M. V. Milošević, and A. Perali, arXiv:2312.09017.